Asian Journal of Chemistry; Vol. 25, No. 16 (2013), 9087-9091

ASIAN JOURNAL OF CHEMISTRY

http://dx.doi.org/10.14233/ajchem.2013.15007

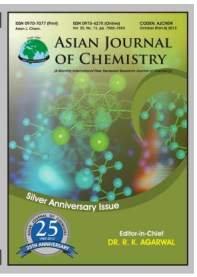

Influences of Pore Sizes on the Catalytic Activity of Fe-MCM-41 in Hydroxylation of Phenol

BING HAN[1,2], XIAOBO SHI[2], YINGJIE ZHANG[2], QINGHU KONG[2], QINGLIN SUN[2] and YAN KONG[2,*]

[1]School of Material Engineering, Nanjing Institute of Technology, Nanjing 211167, P.R. China
[2]China State Key Laboratory of Materials-Oriented Chemical Engineering, Nanjing University of Technology, Nanjing 210009, P.R. China

*Corresponding author: E-mail: kongy36@njut.edu.cn

(*Received*: 24 December 2012; *Accepted*: 18 September 2013) AJC-14119

A series of Fe-MCM-41 with different pore sizes were synthesized by changing alkyl chain lengths of surfactants and the properties of the pore structures were characterized by XRD, BET, TEM and UV-visible techniques. The results show that the pore size, pore volume, a_0 and regularity of Fe-MCM-41 increase as alkyl chain lengths of surfactants increase, while the content and the coordination state of iron species in catalysts remain constant. The pore sizes of Fe-MCM-41s have an important effect on their catalytic activity in the direct hydroxylation of phenol by H_2O_2. The conversion of phenol decreases as the pore sizes become larger, whereas the selectivity of diphenol rises.

Key Words: Fe-MCM-41, Pore sizes, Phenol, Hydroxylation.

INTRODUCTION

Since Mobil corporation firstly used cation surface active agent to successfully synthesize M41S group mesoporous silica in 1992[1,2], these material has attracted many attentions for their high specific surface area (more than 700 $m^2 g^{-1}$), regular pore structure, confined pore size distribution and high thermal stability and thus gains wide application prospects in fields like catalytic and absorbing materials[3,4].

However, deficiency in reactive active sites has greatly restricted the application of pure silica-based mesoporous molecular sieves in catalysis[5-8]. Some researches indicate that when hetero-atoms are introduced into the structure of the mesoporous molecular sieves, the number of active sites and surface acid sites are increased and the redox ability is enhanced, thereby improving its catalytic performance. These days, improved mesoporous molecular sieves are mainly applied in redox reaction, catalytic hydrogenation, polyreaction, condensation, alkylation reaction, isomerization, catalytic cracking reaction, photocatalysis, *etc*.

Benzenediol (catechol, hydroquinone) is an important fine chemical intermediate[9,10]. Catechol is primarily used as intermediates for pesticides and dyes, as well as key intermediates for synthetic perfumes and medicines. In addition, it can be used to produce hair dyes, rubber hardeners, plating bath additives and the like[11,12]. Hydroquinone, primarily employed in areas like sensitized materials, rubber, dye and medicine, can be used as file developer, thermal poly agent for photosensitive resin, antioxidant and intermediates for producing dyes like anthraquinone and azobenzene. Traditional approaches to synthesize hydroquinone are aniline oxidation and diisopropyl benzene oxidation, while catehol is obtained from hydrolysis of materials such as *o*-chlorophenol and *o*-ethoxyphenol[13,14]. Since the 1970s, the catechol-synthesizing method of hydroxylation of phenol using hydrogen peroxide as the oxidant, has gained wide popularity in the research in relation to chemical engineering fields because of its simple process and moderate reaction conditions. Amongst others, the reaction by-product of the hydroxylation of agent, H_2O_2, is less environmentally damaging, easily accessible and more importantly, usable under relatively moderate conditions[15-17].

Nonetheless, since iron is one of the effective activity centers phenol hydroxylation, many iron-based composite oxides and iron-containing molecular sieves have high catalytic performance for the hydroxylation of phenol[18-21]. The results of the previous research conducted by our team showed that Fe-MCM-41 containing more iron is highly catalytic in the hydroxylation of phenol, and at 20 ºC, the conversion rate of phenol can reach 25.3 % and the hydroquinone selectivity is 78.4 %. Compared with other catalysts, hydroxylation of phenol of this kind shows a relatively fast reaction speed at room temperature due to abundant active sites. Meanwhile, the reaction at room temperature will not cause the collapses of the mesoporous molecular sieve pores, *i.e.*, the defect of low hydrothermal stability of the mesoporous molecular sieves can be avoided; furthermore, the energy consumed during production can be

substantially reduced and the hydrogen peroxide is highly efficient and therefore it has a good future for industrial application. However, the selectivity of the product, hydroquinone, is still rather low and cannot meet the requirements in the industrial application. Reactions largely take place in the molecular sieve pores and the reaction performance is solely influenced by the diffusion of the reactant molecules in the pores when the size of the reactant is similar to that of molecular sieve pores. To address this issue, this paper attempts to synthesize a series of mesoporous molecular sieves containing Fe different sizes by selecting templates with different carbon chain lengths, in different aging temperatures and time. This paper also aims to discuss the impact of the size on reaction performance of the hydroxylation of phenol with a view to setting groundwork for industrial amplifier tests.

EXPERIMENTAL

Cetyl alkyl trimethyl ammonium bromide (CTAB), ferric nitrate [$Fe(NO_3)_3 \cdot 9H_2O$], tetramethyl ammonium hydroxide (TMOAH), sodium metasilicate, manufactured by Chemical Reagents of Shanghai Sinopharm Group, Ltd; tetradecyl alkyl trimethyl ammonium bromide (TTAB), dodecyl alkyl trimethyl ammonium bromide (DTAB), bought from Alfa Aesar; octadecyl alkyl trimethyl ammonium bromide (OTAB) bought from Tokyo Chemical Industry Limited; all the chemicals are analytically pure.

Preparing the catalysts: A series of Fe-containing mesoporous molecular sieves of different sizes were synthesized by adopting sol-gel method. 1.9 g of $Na_2SiO_3 \cdot 9H_2O$ and certain templates (1.184 g DTAB/1.4 g CTAB/1.292 g TTAB/1.508 g OTAB) were heated and dissolved in deionized water, and then cooled to room temperature. Different amounts of $Fe(NO_3)_3 \cdot 9H_2O$ were obtained and dissolved into 5 mL deoionized water. The liquid was then put into the above-mentioned mixture and churned actively for 2 h. After that, a certain amount of liquid of tetramethyl ammonium hydroxide was added and the pH value of the liquid was quickly adjusted until it reached 11 by applying 1 mol/L dilute sulfuric acid. The produced sol was then moved into a stainless steel kettle lined with PTFE and the liquid was heated at 100 ºC for 5 days (Fe/Si (molar ratio) = 6/100). The produced sample was then washed centrifugally dried. After this, it was calcined for 5 h at environmental air of 550 ºC (the temperature rising speed in Muffle furnace being 1 ºC/min). The furnace cooling catalyst sample was then marked Cn-Fe-MCM-41 (*n*-standing for the carbon chain length of the template).

Characterization of the catalysts: The X-ray diffraction (XRD) analysis was carried out with the XRD instrument of Rigaku D/Max-RA type: the CuK_α rays ($\lambda = 0.154178$ nm), a Ni filter, a voltage of 40 kV, a current of 40 mA and a test range of $2\theta = 1\text{-}50^\circ$.

The specific surface area and pore size distribution test was conducted with an adsorption instrument of Micromeritics ASAP-2000 type. Before the test, the sample (20-40 accounts) was activated in vacuum for 8 h. And then the specific surface area and the mean pore size were calculated by adopting BET equation and BJH method, respectively.

ICP test was carried out with a spectrometer of Jarrell-Ash 1100 type. The sample was dissolved with hydrofluoric acid and then heated for 5 min. The volume of the cooled sample was fixed using a 20 mL volumetric flask. After that, the Ti-containing quantity was tested. The main test parameters involved are were as follows: cooling air flow of 15 L/min, auxiliary air flow of 0.2 L/min, atomizing air flow of 0.8 L/min, RF power of 1300 W, sampling speed 1.5 mL/min. Besides, all the air used was Argon gas.

Perkin-Elmer Lambda 35 ultraviolet spectrometer was used to obtain UV spectrum, the scanning ranging from 200-600 mm.

Testing the catalyst activity: The test of catalyst activity was carried out in a self-made double-neck glass back which was equipped with water bath of constant temperature, reflux condenser tubes and magnetic stirrer. The typical reaction procedures were as follows: when the temperature of the circulating water in the reactor reached 25 ºC, 0.05 g catalyst was added, followed by 1 g phenol, 15 mL deionized water and 0.37 mL 30 % H_2O_2 (H_2O_2/phenol = 1:3, mole ratio). After 2 h, the liquid was sampled for centrifugal separation. The compositions of products were analyzed using an Agilent 1100 high efficiency liquid chromatography (Chromatographic column: SB-C18). The operating conditions were as follows: mobile-phase methanol-water mixture (methanol/water = 30/70); washing agent: deionized water with a flowing speed of 1 mL/min; column temperature: 30 ºC; sample feeding volume: 5 µL; UV detector $\lambda = 265$ nm. The content of each composition was calculated by adopting external standard method.

RESULTS AND DISCUSSION

Structure and catalytic performance of Fe-MCM-41 synthesized with different templates: Small-angle XRD spectrum is one of the underlying methods for characterizing materials mesoporous structures. Fig. 1 shows the small-angle XRD spectra of calcined Fe-MCM-41 synthesized with different templates. In this figure, A indicates the Fe-MCM-41 synthesized with OTAB template; B stands for the Fe-MCM-41 synthesized with CTAB template; C indicates the Fe-MCM-41 synthesized with TTAB template; D stands for the Fe-MCM-41 synthesized with DTAB template.

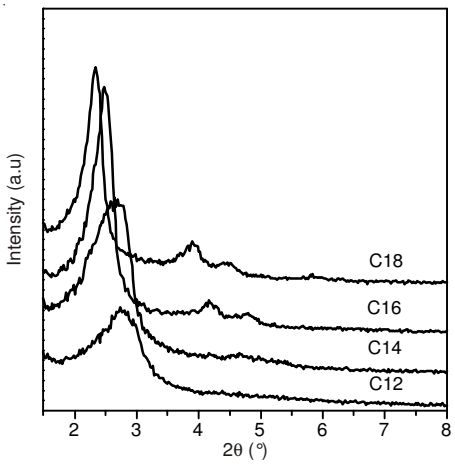

Fig. 1. X-Ray diffraction spectra for Cn-Fe-MCM-41 samples

This figure illustrates that each sample reaches a peak of strong (100) surface diffraction at around 2θ = 2.5º. This is the characteristic peak of a mesoporous molecular sieve, indicating that the synthesized material does have a mesoporous structure. Besides, nearly all the samples have two weaker peaks after the (100) surface diffraction peak, *i.e.*, (110) surface diffraction peak and (200) surface diffraction peak. This indicates that the synthesized material has a MCM-41 hexagonal structure. With the increase in template carbon chain length, the (100) surface diffraction peak shifts towards the small angle, half-peak width apparently becomes smaller and the strength of both the (110) and (200) surface diffraction peaks is also becoming stronger. This means that when the template carbon chain length is increased, a_0 and d_{100} of the mesoporous molecular sieves grow bigger and the hexagonal structure becomes more regular.

Fig. 2 illustrates the N_2 adsorption isotherms of Cn-Fe-MCM-41 samples. From this figure, it can be seen that all isothermal adsorption and desorption lines of the samples are IV isotherms and accompanied by hysteresis loops, which is characteristic of mesoporous molecular sieves[22]. Within the relative pressure range of $0.2 \le P/P_0 \le 0.4$, all isotherms of the samples show transitions. This is caused by the capillary condensation of nitrogen in the pores of mesoporous molecular sieves. Within this pressure range, higher N_2 partial pressure value means larger pore size of the samples; larger transition extent means more regular sample pores and narrower pore size distribution[23]. In Fig. 2, the transition point representing the capillary condensation phase of the isotherm shifts towards bigger relative pressure, which indicates that the pore size is becoming larger with the increase in the template carbon chain length. This result is consistent with the XRD result. Meanwhile, the C12-Fe-MCM-41 sample also has the lowest transition amplitude, that's, the slope, indicating that C12-Fe-MCM-41 is the least regular.

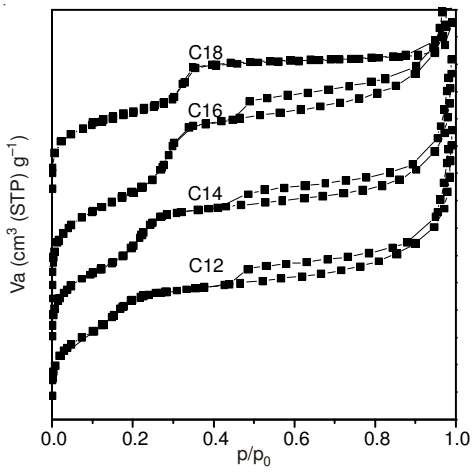

Fig. 2. N_2 adsorption isotherms of Cn-Fe-MCM-41 samples

Fig. 3 illustrates the pore size distribution of Cn-Fe-MCM-41 samples. The pore size is calculated using the BJH method. This figure shows that all samples have a different narrow pore, the regularity is relatively high and the pore size is approximately 2 to 3 nm. With the increasing of the template carbon length, the pore size is apparently becoming larger and the pore volume is also becoming higher. This shows that the sample is becoming increasingly regular.

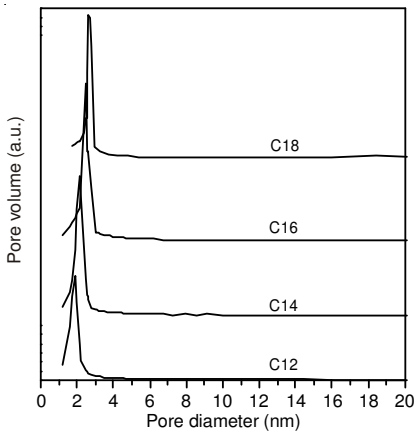

Fig. 3. Pore size distributions of Cn-Fe-MCM-41 samples

Table-1 lists the structure parameters and Fe content of the Cn-Fe-MCM-41 samples. The d_{100} value of the samples can be calculated with the Bragg equation of $\lambda = 2d_{(hkl)} \sin\theta$; since the synthesized material has hexagonal MCM-41 structure, the material lattice parameter a_0 can be estimated with the equation of $a_0 = 2d_{100}/\sqrt{3}$ and the pore wall thickness = a_0-the mean pore size. In this table, the Fe content does not apparently vary with the change of the samples. This means that the change of the template carbon chain length nearly exerts no influence on the Fe content. Nevertheless, the specific surface area, the lattice parameter a_0 and the mean pore size D all regularly vary with the increasing of the template carbon chain length. Based on the figures of the XRD, the N_2 adsorption isotherms and the pore size distribution[24], we can conclude that the micelle size and volume become larger with the increase in the template carbon chain length and thus the mesoporous molecular sieves with larger pore size and volume can be produced.

Fig. 4 illustrates the FT-IR spectra of C16-Fe-MCM-41, before and after being calcined. From this figure, it can be found that the peaks at 2924 and 2844 cm^{-1} points of a curve are caused by C-H bond contraction vibrations, while the b curve does not have such peaks. This indicates that the templates in the mesoporous molecular sieves have been completely removed after being calcined at a high temperature.

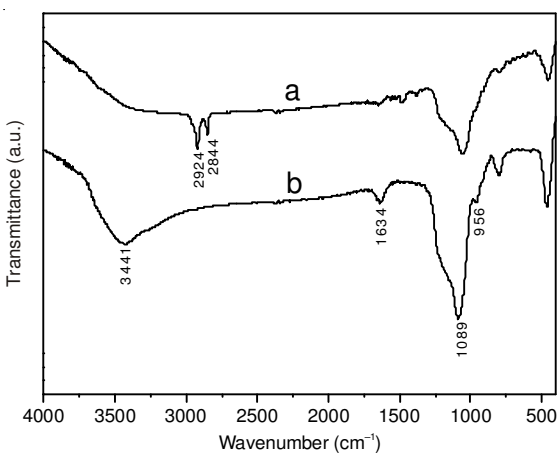

Fig. 4. FT-IR spectra of (a) C16-Fe-MCM-41 as-synthesized, (b) C16-Fe-MCM-41 calcined

TABLE-1
SOME STRUCTURE PARAMETERS OF Cn-Fe-MCM-41 SAMPLES

Sample	nFe/nSi (mol %)[a]		A_{BET} (m^2/g)	V (cm^3/g)	d_{100} (nm)	a_0 (nm)[b]	D (nm)[c]	δ (nm)
	Gel	Product						
C12	0.06	0.059	735	0.79	3.16	3.64	1.89	1.75
C14	0.06	0.061	717	0.85	3.35	3.86	2.11	1.75
C16	0.06	0.062	683	1.04	3.56	4.11	2.44	1.67
C18	0.06	0.062	634	1.37	3.78	4.36	2.70	1.66

Note: a_0 = Lattice constant, A_{BET} = specific surface area, D = pore size, δ = wall thickness V = pore volume. a: ICP results, b: Unit cell parameter value calculated using $a_0 = 2d_{100}/\sqrt{3}$. c: Pore size calculated by BJH method.

Fig. 5 illustrates the UV spectra between 220-800 nm for the calcined Cn-Fe-MCM-41 samples. From this figure, we can find that there is a wide absorption peak between 200-300 nm (centering at 255 nm), caused by d_π-p_π electronic transition of Fe^{3+} ion at the center of iron-oxygen tetrahedron. Since the Fe^{3+} ion is considered as a typical indication that Fe atom exists in the iron-oxygen tetrahedron, the presence of such an absorption peak can fully indicate that the Fe atom has already been introduced into the skeleton of silicon-oxygen tetrahedron of the mesoporous molecular sieves[25,26]. Besides, there is a weak absorption peak between 400 and 500 nm, which probably results from iron-oxygen octahedron and Fe_2O_3 crystal particle[27,28]. This indicates that only a small part of Fe atoms exist in the molecular sieve pores and surface in the format of Fe_2O_3, while most Fe atoms can be synthesized and then introduced into the skeleton of molecular sieves. The UV spectra do not obviously vary with the change of the template carbon chain length during the sample synthesizing. This shows that the changes of templates cannot change the coordination environment of the Fe atoms.

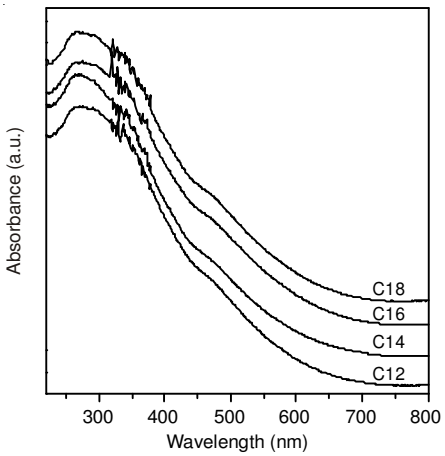

Fig. 5. UV-visible spectra of Cn-Fe-MCM-41 samples

Table-2 shows the catalytic activity of Cn-Fe-MCM-41 during the phenol hydroxylation. With the increase in the template carbon chain length, the conversion rate of phenol gradually decreases from 28.92 to 24.16 %, while the selectivity of hydroquinone rises from 67.83 to 83.86 %. This indicates that catalytic activity of a catalyst depends crucially on the molecular sieve pore size when the catalyst samples have the same Fe content and Fe atom coordination. As the sample pore size increases, the diffusion rate of phenol in the pore becomes higher, giving rise to the decrease in the conversion rate of phenol and rise in the selectivity of hydroquinone. From this table, it can be found that compared with C12-Fe-MCM-41, although the conversion rate of phenol for the C18-Fe-MCM-41 decreases slightly, the selectivity of hydroquinone rises dramatically. As a result, it is an ideal choice to use the C18-Fe-MCM-41 as a catalyst for phenol hydroxylation.

TABLE-2
CATALYTIC ACTIVITY OF Cn-Fe-MCM-41 SAMPLES

Catalyst	Conversion of phenol (%)	Product distribution (%)		
		Diphenol	BQ[b]	nCAT[b]/nHQ[b]
C12	28.02	67.83	1.36	1.69
C14	26.80	74.12	1.45	1.77
C16	25.44	78.74	1.53	1.55
C18	24.16	83.86	1.67	1.52

[a]Reaction conditions: phenol/H_2O_2 = 3:1(molar ratio), 25 ºC, solvent 15 mL H_2O, reaction time 2 h, catalyst/phenol (weight ratio) = 0.05. [b]CAT: catechol; HQ: hydroquinone; BQ: benzoquinone; the rests are tar and oligomer acid.

Conclusion

A series of Fe-MCM-41 with different pore sizes can be synthesized by changing the template carbon chain length. With the increase in the template carbon chain length, the pore size, pore volume, a_0 and regularity of a catalyst can be increased while both Fe content and Fe atom coordination remain unchanged, so its catalytic activity can only be influenced by its pore size. The application of the above-mentioned series of catalysts in the phenol hydroxylation shows that with the increase of pore size, the conversion rate of phenol increases while the selectivity of hydroquinone decreases.

ACKNOWLEDGEMENTS

Thanks to the financial support of National Natural Science Foundations of China (21276125, 20876077), the Support Programs of Jiangsu Province Natural Science Fund (BE2008142), the Jiangsu Province Natural Science Fund (BK2011372) and the Major Projects of the Natural Science Fund for High Education of Jiangsu Province (10KJA530015 and 11KJB430008).

REFERENCES

1. J. Beck, J. Vartuli, W. Roth, M. Leonowicz, C. Kresge, K. Schmitt, C. Chu, D. Olson and E. Sheppard, *J. Am. Chem. Soc*., **114**, 10834 (1992).
2. C. Kresge, M. Leonowicz, W. Roth, J. Vartuli and J. Beck, *Nature*, **359**, 710 (1992).
3. Z.A. Alothman and A.W. Apblett, *Asian J. Chem*., **23**, 514 (2011).
4. A.D. Murkute, J.E. Jackson and D.J. Miller, *J. Catal*., **278**, 189 (2011).
5. J. Okamura, S. Nishiyama, S. Tsuruya and M. Masai, *J. Mol. Catal. A*, **135**, 133 (1998).
6. B. Lindlar, A. Kogelbauer and R. Prins, *Micropor. Mesopor. Mater*., **38**, 167 (2000).
7. B.K. Nath and J.N. Ganguli, *Asian J. Chem.*, **24**, 5292 (2004).

8. Y. Kong, S.Y. Jiang, J. Wang, S. Wang, Q. Yan and Y. Lu, *Micropor. Mesopor. Mater*., **86**, 191 (2005).
9. J. Wang, J.N. Park, H.C. Jeong, K.S. Choi, X.Y. Wei, S.I. Hong and C.W. Lee, *Energy Fuels*, **18**, 470 (2004).
10. R. Alnaizy and A. Akgerman, *Adv. Environ. Res*., **4**, 233 (2000).
11. R. Yu, F.S. Xiao, D. Wang, J. Sun, Y. Liu, G. Pang, S. Feng, S. Qiu, R. Xu and C. Fang, *Catal. Today*, **51**, 39 (1999).
12. M. Maurya, S. Titinchi, S. Chand and I. Mishra, *J. Mol. Catal. A*, **180**, 201 (2002).
13. Y. Jianfeng, Z. Chunlei, Y. Yu, W. Tonghao and S. Chiachung, *Chin. J. Catal*., **18**, (1997).
14. J.F. Yu, Y. Yang, T.H. Wu and C.C. Sun, *Chem. Res. Chin. Univ*., 12 (1996).
15. C. Xiong, Q. Chen, W. Lu, H. Gao and Z. Gao, *Catal. Lett*., **69**, 231 (2000).
16. Y. Yu, Y. Jianfeng, W. Tonghao and S. Chiachung, *Chin. J. Catal*., **18**, 230 (1997).
17. J. Wang, J.N. Park, X.Y. Wei and C.W. Lee, *Chem. Commun*., 628 (2003).
18. J.S. Choi, S.S. Yoon, S.H. Jang and W.S. Ahn, *Catal. Today*, **111**, 280 (2006).
19. S. Kannan, A. Dubey and H. Knozinger, *J. Catal*., **231**, 381 (2005).
20. W. Zhao, Y. Luo, P. Deng and Q. Li, *Catal. Lett*., **73**, 199 (2001).
21. T.M. Suzuki, M. Yamamoto, K. Fukumoto, Y. Akimoto and K. Yano, *J. Catal*., **251**, 249 (2007).
22. F. Qu, G. Zhu, S. Huang, S. Li and S. Qiu, *Chem. Phys. Chem.*, **7**, 400 (2006).
23. P. Llewellyn, Y. Grillet, F. Schüth, H. Reichert and K. Unger, *Micropor. Mater*., **3**, 345 (1994).
24. S. Lim, D. Ciuparu, Y. Chen, Y. Yang, L. Pfefferle and G.L. Haller, *J. Phys. Chem. B*, **109**, 2285 (2005).
25. T. Kawabata, Y. Ohishi, S. Itsuki, N. Fujisaki, T. Shishido, K. Takaki, Q. Zhang, Y. Wang and K. Takehira, *J. Mol. Catal. A*, **236**, 99 (2005).
26. M. Hamdy, G. Mul, J. Jansen, A. Ebaid, Z. Shan, A. Overweg and T. Maschmeyer, *Catal. Today*, **100**, 255 (2005).
27. P.B. Amama, S. Lim, D. Ciuparu, Y. Yang, L. Pfefferle and G.L. Haller, *J. Phys. Chem. B*, **109**, 2645 (2005).
28. A. Vinu, K.U. Nandhini, V. Murugesan, W. Böhlmann, V. Umamaheswari, A. Pöppl and M. Hartmann, *Appl. Catal. A*, **265**, 1 (2004).